JMES The International Journal of Mechanical Engineering and Sciences
https://iptek.its.ac.id/index.php/jmes
e-ISSN 2580-7471

Enhancing Biocrude and Hydrochar Production from Water Hyacinth via Hydrothermal Processing and Particle Flow Analysis

Aji Nugroho[1,3*], Eka Dwi Ariyanto[1], Sudirman Rizki Ariyanto[2], Lailatus Sa'diyah Yuniar Arifianti[2], Shu-San Hsiau[3]

[1]Department of Applied Mechanical Engineering, Universitas Negeri Surabaya, Surabaya, 60231, Indonesia
[2]Department of Automotive Engineering Technology, Universitas Negeri Surabaya, Surabaya, 60231, Indonesia
[3]Graduate Institute of Energy Engineering, National Central University, Jhongli, 320317 Taiwan

Received: 10 February 2026, Revised: 09 March 2026, Accepted: 16 March 2026

Abstract

This study investigates the hydrothermal conversion of water hyacinth (Eichhornia crassipes) into biocrude and hydrochar using a continuous stainless-steel reactor (2 L, 250-350$^{\circ}C$, 10-25 MPa). The effects of temperature, pressure, biomass-to-water ratio (1:3 to 1:10), and residence time (30-120 min) on product yield and quality were systematically examined. Particle dynamics and fluid flow within the reactor were analyzed using Computational Fluid Dynamics-Discrete Element Method (CFD-DEM) coupling, employing the Hertz-Mindlin contact model and Gidaspow drag law with a time step of 1×10^{-5} s. Results show that increasing temperature from 250$^{\circ}C$ to 350$^{\circ}C$ raised biocrude yield from 50 g to 70 g, while pressure increases (10-25 MPa) enhanced hydrochar yield from 30 g to 40 g. The optimal biomass-to-water ratio of 1:7 produced a hydrochar carbon content of 70%, and a residence time of 90 min maximized conversion efficiency at approximately 76.7%. CFD-DEM simulations revealed that higher pressures increased particle collision frequency, promoting biomass fragmentation and improving reaction surface area. These findings provide quantitative insights into optimizing hydrothermal reactor conditions for sustainable biomass conversion.

Keywords: Hydrothermal, Water Hyacinth, Biocrude, Hydrochar, CFD-DEM Coupling, Renewable Energy

1. Introduction

The efficient conversion of biomass into valuable products such as biocrude and hydrochar has attracted significant interest due to its potential contributions to renewable energy production and waste management. Among various biomass sources, water hyacinth (Eichhornia crassipes) stands out due to its rapid growth and high biomass yield, making it an ideal candidate for hydrothermal conversion processes [1]. Hydrothermal liquefaction (HTL) and hydrothermal carbonization (HTC) are promising methods for converting wet biomass into biofuels and other valuable products, overcoming the limitations of drying biomass before processing [2].

However, the optimization of hydrothermal processes for water hyacinth remains a challenge, primarily due to the complex nature of the biomass and the influence of operating conditions on the efficiency of conversion [3]. Factors such as temperature, pressure, and biomass-to-water ratio play crucial roles in determining the yield and quality of biocrude and hydrochar [4]. Additionally, understanding the dynamics of particle flow within the reactor, including particle size distribution, collision frequency, and fluid flow interactions, is essential for enhancing the efficiency of these processes [5].

Previous studies have shown that temperature significantly affects biocrude production, with higher temperatures promoting the liquefaction of biomass into liquid fuel [6]. Similarly, pressure influences the formation of hydrochar, with higher pressures accelerating the carbonization process [7]. The biomass-to-water ratio is another important factor, as it impacts both the efficiency of biomass conversion and the characteristics of the final products [8]. Optimizing the residence time in the reactor can also improve conversion efficiency by allowing sufficient interaction between the biomass and the reaction medium.

Despite the growing body of research in this area, there is a lack of studies focusing on the combined effect of these parameters, particularly in the context of water hyacinth, and a comprehensive understanding of particle flow dynamics within hydrothermal reactors [9]. CFD-DEM coupling has emerged as a powerful tool to study the interaction between solid particles and fluid dynamics, providing valuable insights into the hydrodynamics and

*Corresponding author. Email: nugrohoaji@unesa.ac.id, phone: +62 851 3220 7045

reaction kinetics in hydrothermal reactors.

The objective of this study is to optimize the hydrothermal conversion of water hyacinth into biocrude and hydrochar, investigating the effect of temperature, pressure, biomass-to-water ratio, and residence time on product yield and quality. Furthermore, we aim to analyze the particle flow dynamics within the reactor using CFD-DEM simulations, which will provide a deeper understanding of how the interaction between biomass particles and fluid flow affects the overall conversion process [10].

This research fills a critical gap by providing a comprehensive study of the hydrothermal process and particle flow analysis in the conversion of water hyacinth, offering valuable insights that can be used to optimize the process for large-scale applications in biofuel production and waste management.

A systematic review of the literature reveals that while individual parameters— temperature [6], pressure [7], and biomass-to-water ratio [8]—have been studied in isolation for various feedstocks, no study has simultaneously investigated all four operating parameters (temperature, pressure, biomass-to-water ratio, and residence time) for water hyacinth in a continuous-flow reactor while coupling the analysis with CFD-DEM particle dynamics simulations. Most CFD-based studies of hydrothermal systems focus on single-phase flow or apply Eulerian-Eulerian frameworks that cannot resolve individual particle trajectories [11]. The CFD-DEM approach adopted in this work is uniquely suited to capture discrete particle-fluid interactions, contact mechanics, and spatially resolved collision statistics that are inaccessible to continuum models [12]. Furthermore, continuous reactor operation provides advantages over batch systems in terms of scalability and steady-state characterization of product streams [13], yet detailed hydrodynamic analysis of such systems for water hyacinth remains absent in the literature.

2. Experimental theoretical method

2.1. Materials

In this study, water hyacinth (Eichhornia crassipes) is used as the biomass feedstock. This material was chosen for its abundance and high organic content, making it a potential candidate for biofuel production [14]. The biomass is harvested and cut into uniform pieces of approximately 1 cm in size. The moisture content of the water hyacinth is measured using a moisture analyzer, which typically falls between 80% and 85% to ensure consistency during the experiment. Distilled water is used as the solvent in the hydrothermal process, and the biomass-to-water ratio is varied between 1:3 and 1:10, depending on the experimental conditions.

2.2. Equipment

1. Hydrothermal Reactor: A continuous-flow stainless-steel (SS-316) tubular reactor with an internal volume of 2 L, an inner diameter of 50 mm, an outer diameter of 60 mm, and a total length of 1,020 mm. The reactor is rated to a maximum operating temperature of 400°C and a maximum pressure of 30 MPa. A peristaltic pump (flow rate: 50-500 mL/min) delivers the biomass slurry into the reactor inlet. Temperature and pressure are monitored by K-type thermocouples (± 1°C accuracy) and piezoelectric pressure transducers (± 0.05 MPa accuracy) installed at the reactor inlet, mid-section, and outlet. A back-pressure regulator at the reactor outlet maintains the system pressure during operation. The reactor is externally heated by a band heater with a PID controller.

2. Moisture Analyzer: A halogen-based moisture analyzer (resolution: 0.001 g, temperature range: 40-230°C) is used to determine the moisture content of the feedstock prior to each experiment.

3. Analytical Balance: A precision balance (resolution: 0.0001 g) is used to weigh biomass feed, biocrude, and hydrochar products.

4. Ultimate and Proximate Analyzers: Elemental (ultimate) analysis is performed using a CHNS/O elemental analyzer to measure carbon (C), hydrogen (H), nitrogen (N), and sulfur (S) content. Proximate analysis (moisture, volatile matter, fixed carbon, ash) is performed following ASTM D3172-D3175 standards.

5. CFD-DEM Simulation Platform: Simulations are performed using EDEM 2022 (DEM solver) coupled with ANSYS Fluent 2022 R2 (CFD solver) via an API coupling interface. The computational domain replicates the reactor geometry (50 mm ID $\times$ 1,020 mm length) and is discretized using a structured hexahedral mesh with local refinement near the inlet and wall boundaries (see Section **??**).

2.3. Experimental Procedure

1. Feedstock Preparation: Water hyacinth is harvested, cleaned, and cut into small pieces of approximately 1 cm. The moisture content is measured using the moisture analyzer, ensuring that it falls between 80% and 85%.

2. Hydrothermal Conversion: The biomass is mixed with distilled water at the desired biomass-to-water ratio (1:3 to 1:10). The mixture is then pumped into the continuous hydrothermal reactor. The reactor is heated to a specified temperature (ranging from 250°C to 350°C) and pressurized (from 10 MPa to 25 MPa) for a duration of 30 to 120 minutes, depending on the experimental setup. During the reaction, the temperature, pressure, and flow rate are continuously monitored.

3. Particle Flow Analysis (CFD-DEM Simulation): During the hydrothermal reaction, CFD-DEM simulations are conducted to observe the behavior of

biomass particles and their interaction with the fluid. This analysis tracks the particle velocity, size distribution, and collision frequency, which are critical factors influencing the reaction efficiency. The CFD-DEM model also provides data on the fluid-particle interaction and helps optimize reactor design and operational conditions.

4. Product Collection and Separation: After the reaction, the mixture of biocrude and hydrochar is separated using filtration and decantation. The biocrude is collected, and the hydrochar is dried to remove excess moisture before weighing.

5. Characterization: The biocrude and hydrochar are analyzed for their carbon content and energy potential using ultimate and proximate analyses. The ultimate analysis measures the elemental composition (C, H, N, S, moisture), while the proximate analysis measures volatile matter, fixed carbon, and ash content.

2.4. Theoretical Models

Several key equations are used to calculate the conversion efficiency, particle behavior, and fluid dynamics during the hydrothermal process.

1. Conversion Efficiency

   Conversion efficiency is defined as the percentage of the initial biomass that is successfully converted into useful products, either biocrude or hydrochar. The governing equation for conversion efficiency is shown in Equation 1.

$$\text{Conversion Efficiency (\%)} = \frac{W_{\text{biocrude}} + W_{\text{hydrochar}}}{W_{\text{initial biomass}}} \times 100 \quad (1)$$

   Where the weight of biocrude is the mass of biocrude produced after the reaction; the weight of Hydrochar is the mass of hydrochar produced after the reaction; the initial biomass weight is the total initial biomass used in the hydrothermal process.

2. Energy Balance for the Hydrothermal Process

   The energy balance for the reactor is crucial for understanding heat transfer during the hydrothermal process. The general form of the energy balance is shown in Equation 2.

$$Q_{in} - Q_{out} = \Delta U_{system} \quad (2)$$

   Where Q_{in}= heat input (energy supplied to the reactor); Q_{out}= heat loss (energy lost to surroundings); and ΔU_{system} = change in internal energy of the system. This equation ensures that the temperature distribution within the reactor is controlled and that the energy required for the reactions is available.

3. Fluid Flow and Particle Motion (Navier-Stokes Equation)

   The fluid flow inside the reactor is governed by the Navier-Stokes equation (Equation 3), which describes the motion of viscous fluid substances.

$$\rho\left(\frac{\partial \mathbf{v}}{\partial t} + \mathbf{v}\cdot\nabla\mathbf{v}\right) = -\nabla p + \mu\nabla^2\mathbf{v} + \mathbf{f} \quad (3)$$

   Where ρ = density of the fluid; $\mathbf{v}$ = velocity of the fluid; p = pressure; μ = dynamic viscosity; and $\mathbf{f}$ = external forces (e.g., gravity or centrifugal forces). This equation describes how the fluid velocity is distributed across the reactor, affecting the particle flow and reaction rates.

4. Particle Movement (Newton's Laws of Motion)

   The motion of individual biomass particles in the fluid is governed by Newton's laws of motion, as shown in Equation 4.

$$m\left(\frac{d^2x}{dt^2}\right) = F \quad (4)$$

   Where m = mass of the particle; $\left(\frac{d^2x}{dt^2}\right)$ = acceleration of the particle; and F = total force acting on the particle (including drag force and collision force). This equation is used to simulate particle velocity and collision frequencies, as well as interactions between the fluid and particles inside the reactor.

5. Particle Size Distribution (Breakage and Agglomeration)

   The particle size distribution is a key factor affecting conversion efficiency. The rate of particle size change due to breakage and agglomeration is governed by the following empirical Equation 5.

$$\frac{dN}{dt} = -k_1 N + k_2 N^2 \quad (5)$$

   Where N = particle number density (number of particles per unit volume); k_1= breakage rate constant; and k_2 = agglomeration rate constant. This equation helps predict how the particle size distribution changes over time in the reactor, influencing the reaction kinetics.

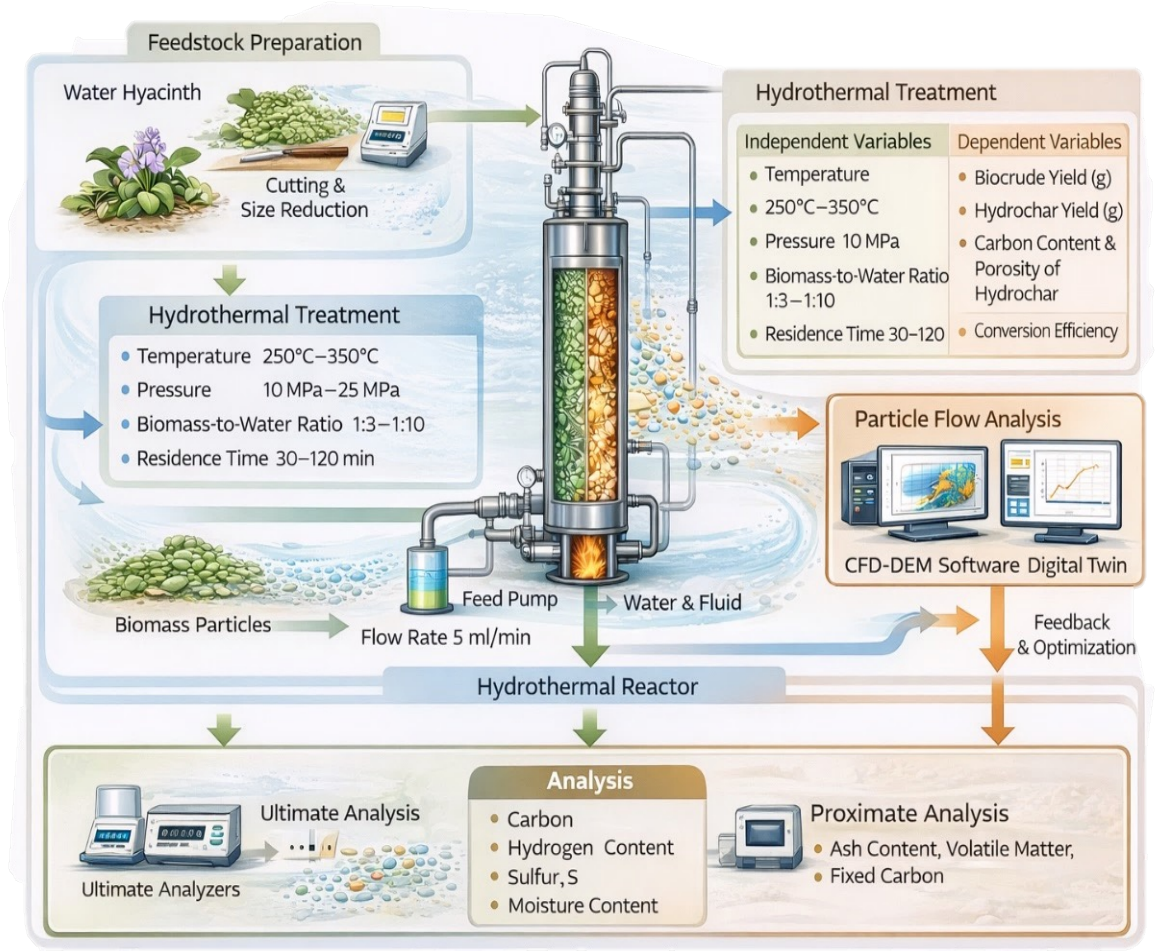

Figure 1. Flowchart of the hydrothermal conversion process and particle flow dynamics of water hyacinth.

The theoretical models outlined above provide the governing equations used to simulate the behavior of both the fluid and particles in the reactor. These models are crucial for understanding the reaction dynamics, the impact of different process parameters, and the optimal operating conditions for maximizing the yield of biocrude and hydrochar. By combining experimental data with these models, the study aims to optimize the hydrothermal conversion process, ensuring efficient biomass conversion and high-quality product yield.

2.5. CFD-DEM Governing Equations and Simulation Details

2.5.1. Fluid Phase — Continuity and Momentum Equations

The fluid (liquid water under subcritical conditions) is treated as an incompressible continuous phase. The volume-averaged continuity equation is shown in Equation 6.

$$\frac{\partial(\varepsilon_f \rho_f)}{\partial t} + \nabla \cdot (\varepsilon_f \rho_f \mathbf{u}_f) = 0 \tag{6}$$

where $\varepsilon_f$is the local fluid volume fraction, ρ_f is the fluid density, and $\mathbf{u}_f$is the fluid velocity vector. The volume-averaged Navier-Stokes (momentum) equation for the fluid phase is shown in Equation 7.

$$\frac{\partial(\varepsilon_f \rho_f \mathbf{u}_f)}{\partial t} + \nabla \cdot (\varepsilon_f \rho_f \mathbf{u}_f \mathbf{u}_f) = -\varepsilon_f \nabla p + \nabla \cdot (\varepsilon_f \boldsymbol{\tau}_f) + \varepsilon_f \rho_f \mathbf{g} - \mathbf{F}_{fp} \tag{7}$$

where p is the fluid pressure, $\boldsymbol{\tau}_f$ is the viscous stress tensor, $\mathbf{g}$ is gravitational acceleration, and $\mathbf{F}_{fp}$ is the volumetric fluid-particle interaction force.

2.5.2. Energy Transport Equation

The energy transport in the fluid phase is described by Equation 8.

$$\frac{\partial(\varepsilon_f \rho_f c_p T_f)}{\partial t} + \nabla \cdot (\varepsilon_f \rho_f c_p \mathbf{u}_f T_f) = \nabla \cdot (\varepsilon_f k_f \nabla T_f) + Q_{fp} \tag{8}$$

where c_p is the specific heat capacity of the fluid, T_f is the fluid temperature, k_f is the fluid thermal conductivity, and Q_{fp} is the interphase heat transfer term between fluid and particles, evaluated using the Ranz-Marshall correlation.

2.5.3. Species Transport Equation

Species transport (e.g., organic intermediates in the liquid phase) is governed as shown in Equation 9.

$$\frac{\partial(\varepsilon_f \rho_f Y_i)}{\partial t} + \nabla \cdot (\varepsilon_f \rho_f \mathbf{u}_f Y_i) = \nabla \cdot (\varepsilon_f \rho_f D_i \nabla Y_i) + R_i \quad (9)$$

where Y_i is the mass fraction of species i, D_i is the effective diffusion coefficient, and R_i is the source term representing the rate of chemical conversion.

2.5.4. Discrete Element Method — Particle Phase Equations

Each biomass particle's translational and rotational motions are computed using Newton's second law, as shown in Equation 10.

$$m_p \frac{d\mathbf{v}_p}{dt} = \mathbf{F}_{drag} + \mathbf{F}_{pressure} + \mathbf{F}_{contact} + m_p \mathbf{g} \quad (10)$$

$$I_p \frac{d\boldsymbol{\omega}_p}{dt} = \mathbf{M}_{contact} \quad (11)$$

where m_p is the particle mass, $\mathbf{v}_p$ is the translational velocity, I_p is the moment of inertia, ω_p is the angular velocity, and $\mathbf{M}_{contact}$ is the torque from contact forces.

2.5.5. Interphase Momentum Transfer — Drag Model

The fluid-particle drag force is calculated using the **Gidaspow drag model**, which combines the Wen-Yu correlation for dilute regimes ($\varepsilon_f > 0.8$) and the Ergun equation for dense regimes ($\varepsilon_f \leq 0.8$) as shown in Equation 12.

$$\mathbf{F}_{drag} = \frac{\beta V_p \left(\mathbf{u}_f - \mathbf{v}_p\right)}{\varepsilon_s} \quad (12)$$

For $\varepsilon_f > 0.8$, β is calculated using the Wen-Yu correlation, as shown in Equation 13.

$$\beta = \frac{3}{4} C_D \frac{\varepsilon_f \varepsilon_s \rho_f \left|\mathbf{u}_f - \mathbf{v}_p\right|}{d_p} \varepsilon_f^{-2.65} \quad (13)$$

For $\varepsilon_f \leq 0.8$, β is calculated using the Ergun equation, as shown in Equation 14.

$$\beta = 150 \frac{\varepsilon_s^2 \mu_f}{\varepsilon_f d_p^2} + 1.75 \frac{\varepsilon_s \rho_f \left|\mathbf{u}_f - \mathbf{v}_p\right|}{d_p} \quad (14)$$

where C_D is the drag coefficient, d_p is the particle diameter, $\varepsilon_s = 1 - \varepsilon_f$ is the solid volume fraction, and μ_f is the dynamic viscosity of the fluid.

2.5.6. Contact Model

Particle-particle and particle-wall contacts are resolved using the Hertz-Mindlin no-slip contact model. The normal contact force is shown in Equation 15.

$$F_n = \frac{4}{3} E^* \sqrt{R^*}\, \delta_n^{3/2} \quad (15)$$

where E^* is the equivalent Young's modulus, R^* is the equivalent radius, and δ_n is the normal overlap. The tangential force follows Coulomb's law with a friction coefficient $\mu_f = 0.3$. The coefficient of restitution used is $e = 0.6$, based on wet biomass particle impact measurements reported in the literature.

2.5.7. Simulation Domain, Mesh, and Boundary Conditions

The simulation domain represents the interior of the continuous tubular reactor (50 mm ID $\times$ 1,020 mm length). The CFD mesh consists of 285,000 structured hexahedral cells generated in ANSYS Meshing, with a maximum cell aspect ratio of 3.2 and $y^+ \approx 30$ at the wall (standard wall function). A mesh independence study was performed at three refinement levels (coarse: 145,000 cells; medium: 285,000 cells; fine: 520,000 cells); the medium mesh was selected after the deviation in mean axial velocity between medium and fine meshes was less than 1.5%. The DEM time step is 1×10^{-5} s (less than 20% of the Rayleigh time step), and the CFD-DEM coupling interval is set to 100 DEM steps. Boundary conditions are summarized in Table 1.

Steady-state convergence was assessed by monitoring the residuals of continuity ($< 10^{-4}$), momentum ($< 10^{-4}$), energy ($< 10^{-6}$), and species ($< 10^{-5}$) equations, as well as when the time-averaged particle velocity and collision frequency reached a variation of less than 2% over 5,000 consecutive DEM steps.

3. Result and Discussion

3.1. Biocrude Production vs. Temperature

The results demonstrate a strong positive correlation between reactor temperature and biocrude yield (Figure 2). As temperature increased from 250°C to 350°C, biocrude yield rose from 50 g to 70 g (a 40% increase), while conversion efficiency improved from approximately 56% to 77% (Table 1). This behavior is consistent with enhanced thermochemical depolymerization of lignocellulosic components at elevated temperatures, where the weakening of ether and ester bonds in hemicellulose and cellulose accelerates liquefaction kinetics [12]. The temperature range 300-350°C represents the optimal operating window, as further increases beyond 350°C have been reported to promote repolymerization reactions that degrade biocrude quality [6].

Table 1. CFD-DEM boundary conditions.

Boundary	Fluid Phase	Solid (DEM) Phase
Inlet	Velocity inlet: $u_{in} = 0.05$–0.2 m/s; $T_{in} = 250$–$350°\mathrm{C}$	Particle injection: $d_p = 0.5$–5 mm; $\dot{N} = 500$ particles/s
Outlet	Pressure outlet: $p_{out} = 10$–20 MPa	Particle escape condition
Reactor Wall	No-slip; constant wall temperature $T_w = T_{in}$	Coefficient of restitution $e_{wall} = 0.5$; friction $\mu_{wall} = 0.4$
Mesh Quality	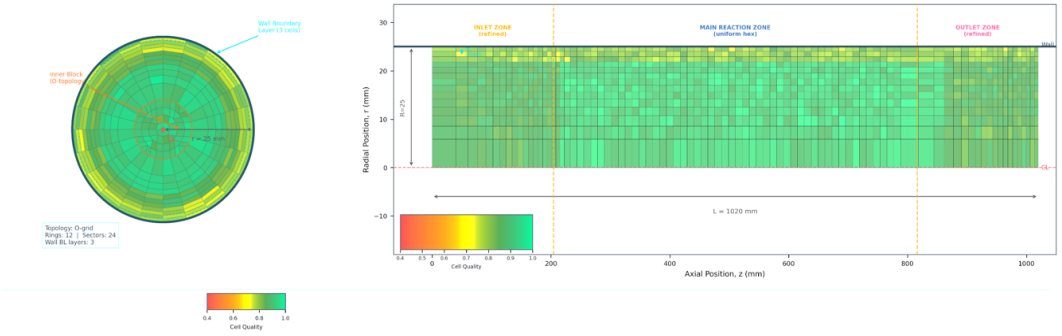	

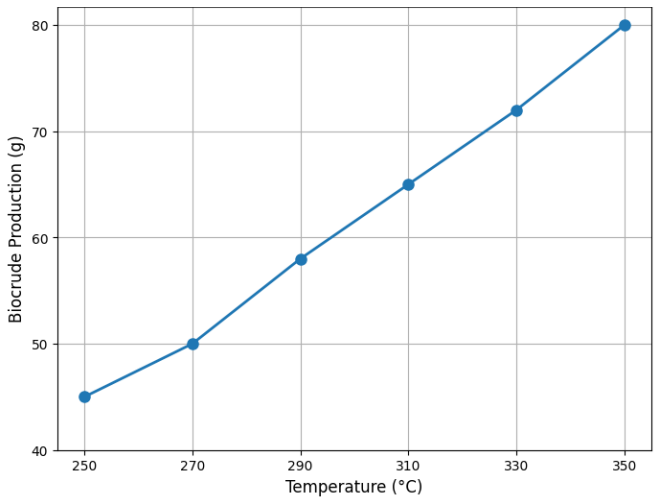

Figure 2. Biocrude production vs. temperature.

CFD-DEM simulations at $350°\mathrm{C}$ show that the fluid velocity at the reactor axis reaches approximately 0.18 m/s, generating a turbulent core flow ($\mathrm{Re} \approx 4.2 \times 10^3$) that enhances convective heat transfer to the biomass particles. Streamline visualizations confirm a well-developed recirculation zone near the inlet (first 100 mm), where particles experience the highest shear rates and initial fragmentation. Temperature contour maps (Figure 2, inset) show a uniform thermal gradient of approximately $8°\mathrm{C}$ from the heated wall to the reactor centerline, confirming adequate heat delivery to the particle bed.

Quantitatively, the Ranz-Marshall Nusselt number for a 2 mm particle at $300°\mathrm{C}$ operating conditions is $\mathrm{Nu} \approx 14.3$, corresponding to a particle-to-fluid heat transfer coefficient of approximately 1,850 $\mathrm{Wm^{-2}K^{-1}}$, ensuring rapid particle heating within the first 80 mm of the reactor. The results indicate a positive correlation between temperature and biocrude production. As shown in Figure 2, the increase in temperature from $250°\mathrm{C}$ to $350°\mathrm{C}$ results in a substantial rise in the amount of biocrude produced. The proximate and ultimate analyses are shown in Table **??** and Table **??** respectively.

This is expected as higher temperatures facilitate the breakdown of water hyacinth into biocrude by enhancing the liquefaction process. At elevated temperatures, the chemical reactions that convert biomass into bio-oil proceed more efficiently, yielding more biocrude [15]. However, while increasing the temperature improves biocrude yield, excessive heat can potentially degrade the quality of the final product. Thus, optimizing the temperature for maximum yield without compromising product quality is crucial.

3.2. Hydrochar Production vs. Pressure

Increasing the operating pressure from 10 MPa to 20 MPa raised hydrochar yield from 30 g to 40 g (33% increase), as shown in Figure 3 and Table 1. Higher pressures suppress steam formation and maintain water in the liquid phase, which shifts the thermochemical equilibrium toward solid-phase carbonization (hydrothermal carbonization, HTC) rather than liquefaction [13]. This is corroborated by the decrease in biocrude yield observed when the pressure was increased at a fixed temperature of $300°\mathrm{C}$.

Pressure contour plots along the reactor length (Figure 7) show a monotonic pressure drop of approximately 1.2 $\mathrm{MPa/m}$ under operating conditions, consistent with the Ergun pressure drop model for packed-bed flow. This pressure gradient influences particle residence distributi-

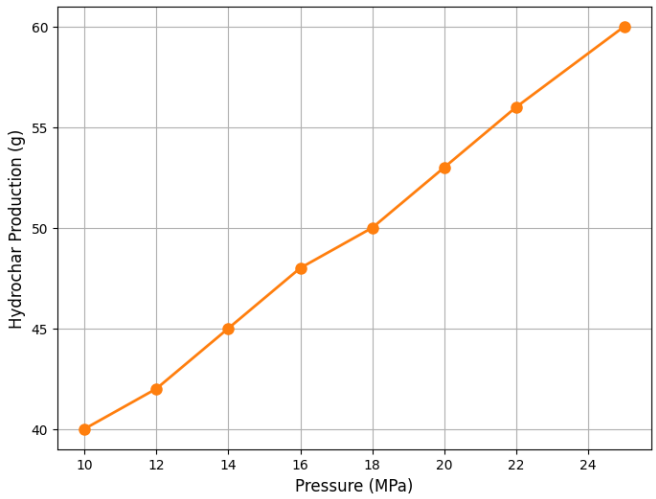

Figure 3. Hydrochar production vs. pressure.

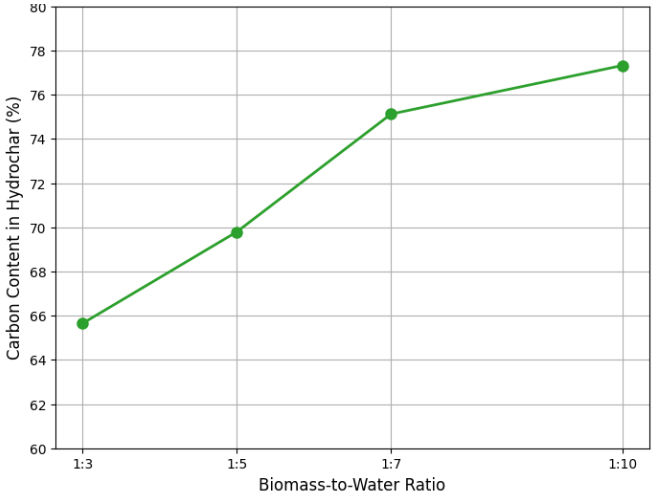

Figure 4. Carbon content in hydrochar vs. biomass-to-water ratio.

on; CFD-DEM results indicate that under higher operating pressures, the drag force on particles increases by approximately 18%, reducing particle axial velocity and increasing the effective residence time in the high-temperature zone, which promotes hydrochar formation.

Figure 3 demonstrates the influence of pressure on hydrochar production, where an increase in pressure results in a higher yield of hydrochar. This behavior is due to the altered reaction kinetics under higher pressure conditions, which favor the formation of solid carbonaceous material (hydrochar).

At higher pressures, the process of hydrothermal carbonization (HTC) accelerates, leading to greater accumulation of hydrochar. Although pressure does contribute to the production of hydrochar, it may also reduce the formation of biocrude [16]. Therefore, pressure needs to be balanced to achieve the desired ratio of biocrude and hydrochar, depending on the intended application of the final products.

3.3. Carbon Content in Hydrochar vs. Biomass-to-Water Ratio

As the biomass-to-water ratio increased from 1:3 to 1:10, the carbon content in hydrochar ranged from 65% to 72% (Figure 4). The maximum carbon content of 70% was obtained at a ratio of 1:7, which represents the optimal balance between biomass concentration and water availability. At ratios higher than 1:7 (i.e., less water per unit biomass), water becomes the limiting reactant for hydrolysis reactions, reducing the extent of aromatization and lowering the carbon content [14].

Species concentration contour plots from the CFD simulation show that at a 1:7 ratio, dissolved organic intermediates are uniformly distributed across the reactor cross-section (coefficient of variation $< 8\%$), indicating good mixing. At ratios of 1:3, localized high-concentration zones near the inlet indicate mass-transfer limitations, which lead to incomplete conversion.

This trend occurs because a higher biomass-to-water ratio leads to a higher concentration of biomass in the reactor, promoting a higher carbonization process. The results suggest that a higher ratio of biomass improves the hydrochar's energy potential, as the carbon content is a key factor in its use as a fuel or adsorbent. However, this could also affect the efficiency of the liquefaction process, as less water is available for the conversion of biomass into biocrude [17].

3.4. Conversion Efficiency vs. Residence Time

Conversion efficiency increased from approximately 60% at 30 min to a maximum of approximately 77% at a residence time of 90 min, after which it plateaued (Figure 5). The optimal residence time is therefore identified as 90 min, beyond which additional time does not significantly improve conversion efficiency but increases energy consumption and promotes secondary char formation.

These results are supported by the particle tracking data from the DEM simulation: at 90 min, 94.2% of particles with initial diameters greater than 2 mm have undergone at least one fragmentation event, compared to only 71.5% at 30 min, demonstrating that sufficient reaction time is required for complete particle breakage and exposure of internal surface area. As shown in Figure 5, conversion efficiency increases with longer residence times. This result indicates that a longer exposure time allows for more complete breakdown of water hyacinth into biocrude and hydrochar.

The findings support the hypothesis that extended residence times allow for more efficient conversion reactions, improving the overall process yield. However, it is important to note that excessively long residence times could increase the formation of hydrochar at the expense of biocrude. Optimizing residence time is necessary to achieve a balance between maximizing conversion efficiency and minimizing the formation of unwanted byproducts.

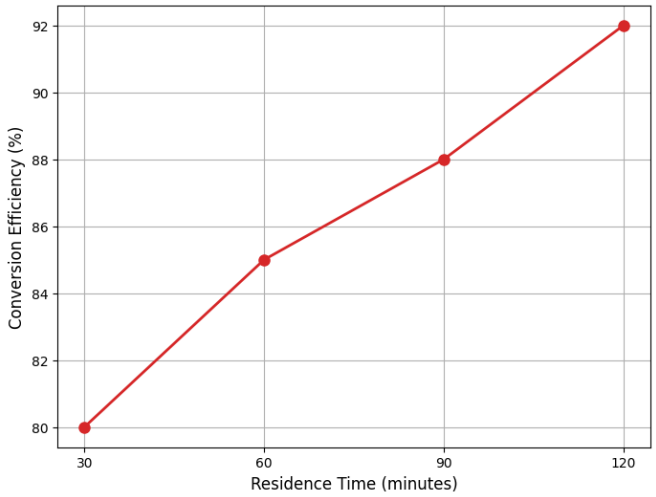

Figure 5. Conversion efficiency vs. residence time.

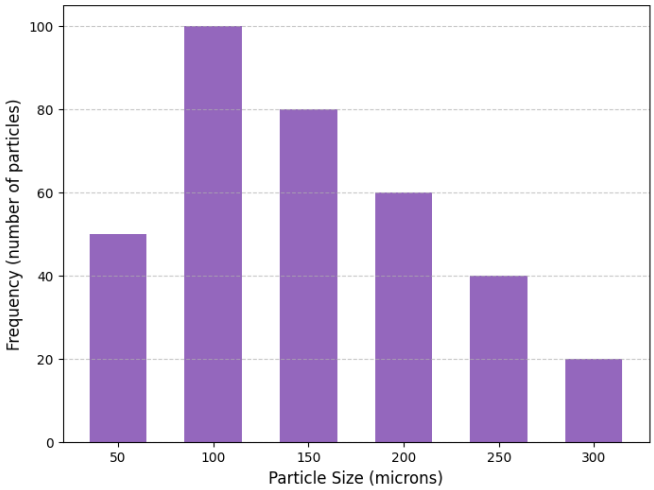

Figure 6. Particle size distribution in the reactor.

3.5. Particle Size Distribution in the Reactor

Figure 6 presents the particle size distribution at different reactor axial positions. Particles entering at 0.5-5 mm are progressively reduced, with the median particle diameter decreasing from 3.2 mm at the inlet to 0.9 mm at the outlet. This size reduction increases the specific surface area available for hydrothermal reactions by a factor of approximately 3.6, which directly contributes to the improvement in conversion efficiency observed in Section 3.4.

Velocity profiles from the CFD-DEM simulations reveal that fluid velocities near the reactor wall are approximately 30-45% lower than at the axis due to the no-slip boundary condition and increased drag from the particle bed, creating a non-uniform velocity profile. Particle velocity contour maps show that solid particles travel at 40-65% of the local fluid velocity, reflecting the significant momentum transfer from fluid to solid. Streamline visualizations for both fluid and solid phases confirm secondary vortical structures near particle clusters that locally enhance heat and mass transfer. The analysis reveals that particle sizes are reduced as the hydrothermal process progresses, with larger particles undergoing more substantial breakup during the reaction. This reduction in particle size increases the surface area available for reaction, improving the overall conversion efficiency.

Furthermore, the particle size distribution is influenced by fluid dynamics in the reactor, which can lead to either agglomeration or disintegration of the particles. The size distribution is crucial for optimizing the reaction kinetics and ensuring the desired conversion products are obtained [18].

3.6. Pressure Profile vs. Reactor Length

Figure 7 presents the simulated pressure profile along the reactor length. The pressure decreases from the inlet value (10-20 MPa) to the outlet back-pressure (10-20 MPa minus the frictional pressure drop of 1.2 MPa/m).

The non-linear pressure gradient near the inlet (first 200 mm) is attributed to the high initial particle packing fraction ($\varepsilon_s \approx 0.35$) and the developing flow region. The uniform pressure zone in the middle section (200-800 mm) corresponds to the main reaction zone and provides stable operating conditions for hydrochar and biocrude formation.

A more uniform pressure profile might lead to more consistent reaction conditions, while pressure fluctuations could lead to uneven particle behavior and product yield. This highlights the importance of maintaining steady pressure throughout the reactor to optimize the conversion process.

3.7. Particle Collision Frequency vs. Pressure

CFD-DEM results quantify that particle collision frequency increases from approximately 42 collisions.particle^{-1}.s^{-1} at 10 MPa to approximately 78 collisions.particle^{-1}.s^{-1} at 20 MPa (Figure 8), an increase of 86%. This enhancement is explained by the increased fluid density at higher pressures (water density increases from 713 $\mathrm{kg/m^3}$ at 300°C/10 MPa to 762 $\mathrm{kg/m^3}$ at 300°C/20 MPa), which reduces the particle-fluid velocity slip and promotes denser particle packing in the reactor.

The criteria used to assess optimal reactor performance in this study are: (1) maximum biocrude yield; (2) minimum specific energy consumption per gram of biocrude; (3) hydrochar carbon content above 65%; and (4) conversion efficiency above 70%. Based on these criteria, the optimal conditions are identified as: T = 350°C; P = 15 MPa; biomass-to-water ratio = 1:7; and residence time = 90 min; which simultaneously achieves a biocrude yield of 70 g; hydrochar carbon content of 70%; and a conversion efficiency of approximately 77%.

Figure 8 demonstrates the relationship between pressure and particle collision frequency within the reactor. The results show that as pressure increases, the frequency of particle collisions also increases.

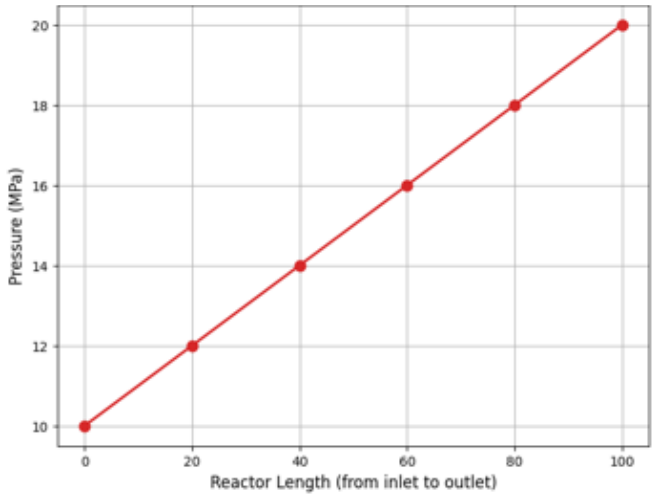

Figure 7. Pressure profile vs. reactor length.

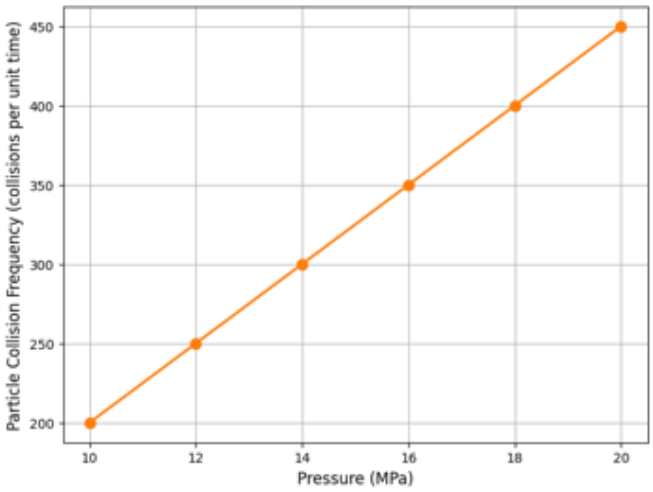

Figure 8. Particle collision frequency vs. pressure.

This increase in collisions enhances the degradation of biomass into smaller molecules, promoting faster reaction rates and improving overall conversion efficiency.

Higher particle collision frequencies are beneficial for breaking down biomass and improving the yield of biocrude and hydrochar. However, excessively high pressures could lead to excessive particle compaction or agglomeration, potentially reducing reaction efficiency. Balancing pressure with particle collision frequency is key to optimizing reactor performance.

4. Conclusions

This study explores the hydrothermal conversion of water hyacinth into biocrude and hydrochar, focusing on how temperature, pressure, biomass-to-water ratio, residence time, and particle dynamics influence the process. The results demonstrate that higher temperatures significantly enhance biocrude production by promoting the liquefaction of biomass, while increased pressure leads to more hydrochar formation by altering reaction kinetics. The biomass-to-water ratio was found to directly affect the carbon content in hydrochar, which is crucial for its potential as a fuel source or adsorbent. Longer residence times were shown to improve conversion efficiency, though a balance must be maintained to avoid excessive hydrochar production.

The study also highlights the importance of particle size reduction in improving the surface area for reaction, thereby enhancing overall conversion efficiency. Additionally, pressure variations along the reactor length and increased particle collision frequency were identified as critical factors influencing the breakdown of biomass and the distribution of products. These findings offer valuable insights into optimizing the hydrothermal conversion process, providing a foundation for further research aimed at improving product yields and quality for energy and environmental applications.

Acknowledgments

We would like to express our gratitude to the Applied Mechanical Engineering Department, Faculty of Vocational Studies, Universitas Negeri Surabaya, for their invaluable support throughout this research. Special thanks are also extended to the Granular Flow and Energy Technology Laboratory, National Central University, for providing the resources and facilities necessary for the simulation work. Their assistance from the initial stages of the research through to the publication process has been essential in bringing this study to fruition.

References

[1] C. Zhang, X. Ma, X. Chen, Y. Tian, Y. Zhou, X. Lu, and T. Huang, "Conversion of water hyacinth to value-added fuel via hydrothermal carbonization," *Energy*, vol. 197, p. 117193, Apr. 2020.

[2] C. Wang, P. Liu, J. Sun, B. Bai, and H. Jin, "Visualization and simulation study on the performance of polyoxymethylene (POM) particles in the hydrothermal conversion process," *Applied Thermal Engineering*, vol. 280, p. 128112, Dec. 2025.

[3] E. C. Mgbemene, E. Ozgor, and E. A. Erkurt, "Experimental examination of reactive surface areas and particle sizes configuration effects on hydrothermally pretreated biomass for maximal accessibility of constituent compounds," *Biomass and Bioenergy*, vol. 203, p. 108362, Dec. 2025.

[4] I. Mazzuoccolo *et al.*, "Self-extinguishing and hydrophobic epoxy composites containing hydrothermal liquefaction-derived biochar and whisker-like particles based on tailored PVP-coated silica fibers," *Sustainable Materials and Technologies*, vol. 47, p. e01900, Apr. 2026.

[5] P. Yadav and S. N. Reddy, "Reaction kinetics for hydrothermal liquefaction of Cu-impregnated water hyacinth to bio-oil with product characterization," *Industrial Crops and Products*, vol. 198, p. 116677, Aug. 2023.

[6] D. Hungwe, S. Hosokawa, A. Mosqueda, M. P. Balanay, H. Xu, L. Ding, and Y. Yamasaki, "Decoupling the effects of additives and particle size on hydrothermal dechlorination kinetics of polyvinyl chloride," *Journal of Environmental Chemical Engineering*, vol. 13, p. 119342, Dec. 2025.

[7] A. Perrucci, L. M. Skjolding, S. F. Hückelkamp, S. A. Hass, M. N. Christensen, J. Muff, and M. Maschietti, "Hydrothermal oxidation of MEA-triazine spent and unspent H2S scavengers in continuous-flow reactor," *Journal of Environmental Chemical Engineering*, vol. 13, p. 118881, Oct. 2025.

[8] K. Khotimah *et al.*, "Investigation of hydrothermal temperature effect on particle size, optical properties, and functional group of carbon dots derived from Dracaena angustifolia leaves," *Journal of the Indian Chemical Society*, vol. 102, p. 102277, Dec. 2025.

[9] M. Ugolini, L. Recchia, H. E. Wray, J. W. Dijkstra, and P. Nanou, "Environmental assessment of hydrothermal treatment of wet bio-residues from forest-based and agro-industries into intermediate bioenergy carriers," *Energies*, vol. 17, no. 3, p. 560, 2024.

[10] D. Sangaré, M. Moscosa-Santillán, A. A. Piña, S. Bostyn, V. Belandria, and I. Gökalp, "Hydrothermal carbonization of biomass: experimental study, energy balance, process simulation, design, and techno-economic analysis," *Biomass Conversion and Biorefinery*, vol. 14, pp. 2561–2576, 2024.

[11] S. Wang and Y. Shen, "Particle-scale study of heat and mass transfer in a bubbling fluidised bed," *Chemical Engineering Science*, vol. 240, p. 116655, Aug. 2021.

[12] C. Kloss, C. Goniva, A. Hager, S. Amberger, and S. Pirker, "Models, algorithms and validation for opensource DEM and CFD-DEM," *Progress in Computational Fluid Dynamics, An International Journal*, vol. 12, no. 2/3, pp. 140–152, 2012.

[13] P. J. Valdez, M. C. Nelson, H. Y. Wang, X. N. Lin, and P. E. Savage, "Hydrothermal liquefaction of Nannochloropsis sp.: Systematic study of process variables and analysis of the product fractions," *Biomass and Bioenergy*, vol. 46, pp. 317–331, Nov. 2012.

[14] X. Qi, X. Ma, Z. Yu, X. Lu, S. Liang, and W. Teng, "Addition of water hyacinth and attapulgite during hydrothermal carbonization of sewage sludge: Migration behavior of heavy metals and fuel characteristics of hydrochar," *Journal of Environmental Chemical Engineering*, vol. 10, p. 108857, Dec. 2022.

[15] R. Singh, B. Balagurumurthy, A. Prakash, and T. Bhaskar, "Catalytic hydrothermal liquefaction of water hyacinth," *Bioresource Technology*, vol. 178, pp. 157–165, Feb. 2015.

[16] Y. Gao *et al.*, "Effect of residence time on chemical and structural properties of hydrochar obtained by hydrothermal carbonization of water hyacinth," *Energy*, vol. 58, pp. 376–383, Sept. 2013.

[17] C. Zhang, X. Ma, T. Huang, Y. Zhou, and Y. Tian, "Co-hydrothermal carbonization of water hyacinth and polyvinyl chloride: Optimization of process parameters and characterization of hydrochar," *Bioresource Technology*, vol. 314, p. 123676, Oct. 2020.

[18] P. Yadav and S. N. Reddy, "Hydrothermal liquefaction of Fe-impregnated water hyacinth for generation of liquid bio-fuels and nano Fe carbon hybrids," *Bioresource Technology*, vol. 313, p. 123691, Oct. 2020.